Applied Surface Science 730 (2026) 166323

Contents lists available at ScienceDirect

Applied Surface Science

journal homepage: www.elsevier.com/locate/apsusc

Full Length Article

High-quality fs-laser structured Si in air for optoelectronic applications

Rafael Benítez-Fernández [a,*], Gonzalo Gomez-Munoz [b], Eric García-Hemme [a], Núria Roca–Giménez [a], Fátima Cabello [b], Marina García-Pardo [b], Jose Gonzalo [b], Javier Solis [b], Álvaro del Prado [a], Mario Garcia-Lechuga [b], Javier Olea [a], Jan Siegel [b], David Pastor [a]

[a] Dpto. EMFTEL, Univ. Complutense de Madrid, Fac. de CC. Físicas, 28040 Madrid, Spain
[b] Laser Processing Group, Instituto de Óptica "Daza de Valdés" (IO), CSIC, Serrano 121, 28006 Madrid, Spain

ARTICLE INFO

Keywords:
Femtosecond laser irradiation
High aspect-ratio micro-structured silicon
Rapid thermal annealing
Silicon oxide removal
High photon absorption

ABSTRACT

In this work, we describe a methodology to highly improve the quality of micro-structured silicon obtained by femtosecond-laser irradiation in ambient air atmosphere. Optimum femtosecond laser irradiation conditions have been selected to obtain a high aspect ratio spike morphology at the surface of silicon. Due to the aggressive fs-laser process, the crystalline structure of the material presents extended defects, which can be removed by rapid thermal annealing. Moreover, thermal annealing triggers diffusion of oxygen to the surface, which was incorporated from the air atmosphere into the bulk upon repetitive fs-laser irradiation. This oxygen binds with silicon atoms within the amorphous surface layer, giving rise to SiOx, obtaining irregular decorations at the surface of the spike structures. These decorations can be removed by a buffered hydrofluoric acid solution, which etches the silicon oxide but not the crystalline silicon. Using this strategy we have obtained a high crystalline quality with: high absorption of around 95 % in the wavelength region from 200 to 1100 nm, minimized defect-related absorption from 1100 to 2500 nm; a crystalline lattice free of defects and oxygen; and a high aspect-ratio micro-spike morphology formed by c-Si free of surface SiO_x nano-decorations that can be useful to fabricate optoelectronic devices.

1. Introduction

Since the first reported study about micro-structured silicon by fs-laser processing for enhanced light absorption [1], a large amount of work has been published in different fields such as photovoltaics [2–4], surface wetting [5], or near-infrared (NIR) and ultraviolet (UV) photodetection [6], among others [7]. Although the texturing process is well-known in the photovoltaic industry to reduce the light reflectance, it has been historically performed using wet etching with chemical reactants like NaOH, KOH or TMAH. However, the typical minimum reflectance reached by wet etching is around 10 % in the wavelength range from 400 to 1000 nm [8], and lower values are only achievable with extra antireflecting coatings that only can be optimized for narrow wavelength ranges [9]. In contrast, laser texturing has enables reflectance values below 5 % in all the visible range [10]. Moreover, the use of solutions which contain alkaline elements contributes to the contamination of the silicon substrate, since these elements act typically as carrier recombination centers [11], such that the substrate needs a subsequent cleaning to eliminate the contaminating elements [12]. Laser micro-structuring does not require any chemical reactant, so no alkaline elements are incorporated into the material. Laser processing is often done in a controlled atmosphere of SF_6 with the intention of incorporating sulfur as a deep impurity center [10], to facilitate the absorption of photons with energies below the silicon bandgap through an extrinsic defects mechanism [13], whereas fluorine greatly contributes to the texturing process via etching. Other studies have been carried out in several gas atmospheres such as N_2 [14], Cl_2 [1,14], air [14–16], or even vacuum [17]. Some studies have been carried out also in water [18]. There are two main reasons to perform laser processing in an ambient air atmosphere: (1) simplicity (no vacuum chamber and careful pressure control are needed) and (2) absence of non-controlled contaminants (no intended impurities, apart from the elements from the air, can be incorporated into the material). Thus, fs-laser processing in ambient air can easily be incorporated in a typical manufacturing route of optoelectronics devices in order to enhance light absorption. Moreover, as an additional advantage, fs–laser microtexturing is an

* Corresponding author.
E-mail addresses: rafaeben@ucm.es (R. Benítez-Fernández), dpastor@ucm.es (D. Pastor).

https://doi.org/10.1016/j.apsusc.2026.166323
Received 15 December 2025; Received in revised form 31 January 2026; Accepted 12 February 2026
Available online 21 February 2026

environmentally friendly process due to the lack of chemical reactants, most of which are toxic and contaminant and require complex procedures for use and disposal.

In a previous publication [19], we reported a detailed study on how different fs-laser processing conditions in ambient air affected the morphology and periodicity of fs-laser induced microstructures in silicon. Optimal texturing conditions were selected from the analysis of optical and morphological results assuring the highest light absorption (over 94 % above the 1.12 eV silicon bandgap ($\lambda = 1100$ nm)) and aspect ratio of the structures. In addition, the material obtained showed a significant light absorption below bandgap. As far as the laser processing route followed to texture the semiconductor samples inly considered the irradiation in ambient air, not intended impurities were inserted in the Silicon lattice to improve the material absorption of photons below the bandgap [20]. Due to this absence of deep level impurities, the $>$ 20 % subbandgap absorptance shown by the as-processed material was partly attributed to defects in the material induced by the aggressive laser irradiation [20–23]. Moreover, the silicon surface shows a kind of irregular structures that "decorate" the spikes [19], which can affect the subsequent steps to fabricate an optoelectronic device. Pulsed laser melting (PLM) was performed in order to remove these defects. However, the decrease in the sub-bandgap absorptance after PLM was only slight. This result indicates that the induced defects are not superficial but deep, so PLM was not able to remove all of them. A rapid thermal annealing (RTA), which is able to remove the defects in the bulk, was performed. The resulting absorptance spectrum showed a noticeable decrease in the 1100 to 2500 nm range, reaching a stable value of around 20 %. Similar results have been reported in other works [24,25], attributing this 'absorptance' to an artifact in the spectrophotometry measurements due to the geometry of the spike structures, enhancing the coupling and trapping of incident light in a way that the light can escape around the edges of the substrate [25,26].

Moreover, due to the composition of the air atmosphere, impurities like oxygen or nitrogen are incorporated into the material during the fs-laser process [14]. In the case of oxygen, this effect is also observed even when the fs-laser process is performed in a controlled atmosphere like SF_6, H_2 or vacuum [14]. Thus, this oxygen incorporation is not only due to the atmosphere composition but also to the native oxide layer at the silicon surface [27]. In our case, we have previously reported around 30 % at. concentration of oxygen in micro-structured silicon surface by energy dispersive X-ray microanalysis (EDX) measurements [19]. This oxygen can be part of the deep defects in the material and could have deleterious effects on the optical and electrical properties, so it would be desirable to remove it.

In this work, we analyze the effect of the RTA post processing on the structural, crystallinity, compositional and optical properties of the structures and how these properties can be improved by removing the defects induced in the fs-laser process, in particular the crystalline defects and the oxygen incorporation. The results presented in this work refer to material-level structural, compositional and optical properties, and are intended to support future integration of fs-laser-textured silicon into optoelectronic devices rather than to demonstrate device performance. The proposed RTA-BOE process yields a microstructured silicon surface with high optical absorptance and improved material quality, suitable as a starting platform for subsequent device fabrication steps for applications in the visible range such as solar cells with minimal modification of the manufacturing route, or further enhanced via hyperdoping techniques, for IR applications. While our previous work focused on optimizing femtosecond-laser parameters to tailor the morphology and optical response of black silicon fabricated in air, the present study goes beyond morphological optimization by addressing the structural and chemical limitations of the laser-processed material. In particular, we provide direct evidence of extended crystalline defect removal throughout the microstructures by rapid thermal annealing, elucidate annealing-induced oxygen redistribution toward the surface, and introduce a selective oxide removal step to obtain a clean crystalline microstructured silicon surface. This combined analysis and process strategy was not addressed in the previous study and is essential for improving material quality and enabling subsequent optoelectronic applications. The results presented in this work refer to material-level properties and are intended to support future device integration rather than to demonstrate photovoltaic device performance.

2. Experimental

Double-side polished, boron-doped, p-type (100) prime CZ-Si wafers with 500 ± 15 μm thickness and resistivity between 1 and 10 Ω·cm were processed in areas of 1.1×1.1 cm^2 with a fs-laser in ambient air conditions, with an energy fluence of 1.4 J/cm^2, an effective pulse number of 700 pulses, and a pulse repetition rate of 300 kHz. These are the optimal conditions of crystallinity, aspect ratio and absorption determined in the previous study [19]. The laser source used is an Yb-doped fiber laser (Satsuma HP, Amplitude Systemes) operating at a central wavelength of 1030 nm, with a pulse duration of 290 fs and a maximum pulse repetition rate of 500 kHz that can be varied within the 1 – 500 kHz interval. The scanning system is composed of a galvanometric scanner (ScanCube 14, Scanlab) and a F-Theta lens (f = 254 mm), deflecting the focused laser beam over the stationary silicon wafer surface. The beam polarization was linear (vertical on the sample) and perpendicular to the scanning direction. The spot diameter at the sample surface of the Gaussian-shaped laser beam was determined following the method proposed by Liu to be $2\omega_0 = 46$ μm ($1/e^2$ intensity) [28], where ω_0 is the spot radius. The setup was also equipped with a tube for air suction to remove the dense fume that is produced during the laser irradiation. To increase the crystallinity a RTA processing step was carried out at 1000 °C during 2 min in a MPTC RTP 600 model system with a controlled Ar atmosphere; this condition was selected to ensure complete recovery of extended crystalline defects, while a systematic optimization of annealing parameters is beyond the scope of this work. The RTA sources are 21 incandescent tungsten lamps (10 on the top and 11 on the bottom). The power of each lamp is 1 kW. Finally, to remove the incorporated oxygen, BOE (Buffered Oxide Etch) etchings at room temperature were done with a commercial buffered hydrofluoric acid BOE 7:1 ($HF : NH_4F = 12.5 : 87.5$ %) that acts as a silicon oxide selective etchant.

To increase the crystallinity, a rapid thermal annealing (RTA) step was carried out at 1000 °C for 2 min in a MPTC RTP 600 system under a controlled Ar atmosphere; this condition was selected to ensure complete recovery of extended crystalline defects, while a systematic optimization of annealing parameters is beyond the scope of this work. The RTA sources are 21 incandescent tungsten lamps (10 on the top and 11 on the bottom), each with a power of 1 kW.

To analyze the crystal quality of the samples, Raman spectroscopy measurements were carried out at room temperature in the backscattering configuration. A dispersive confocal NT-MDT NTegra Spectra micro-Raman microscope equipped with a green laser (532 nm) was used.

In order to analyze the crystal structure and chemical composition of the as-fabricated spikes and the effects of the RTA on them, cross section lamellas of the spikes structure, both before and after the annealing, were fabricated by focused ion beam (FIB) for cross section transmission electron microcopy (TEM) and High-Resolution TEM (HRTEM) analysis.. The lamellas were prepared following a standard FIB lift-out procedure and subsequently thinned to electron transparency, with final polishing steps performed at low ion energies to minimize beam-induced damage. The lamellas were fabricated using a Ga^+ beam from a Fischione Ionic Thinner model 1010.

Cross section-TEM images were taken using a JEOL JEM 3000F with an accelerated voltage of 300 kV and a resolution of 0.17 nm. This microscope is equipped with a GATAN ADF detector for scanning transmission electron microscopy (STEM) mode with a resolution of 0.14 nm, a high-angle annular dark field (HAADF) detector for the acquisition of

Z-contrast images, and an Energy dispersive X-ray (EDX) microanalysis system OXFORD XPLORE. Electron diffraction patterns (ED) of different regions in the spikes were also obtained with this equipment.

Scanning electron microscopy (SEM) images were taken with a JEOL 7600F SEM in order to observe the effects of the BOE etching on the samples surface. The SEM is equipped with an INCA EDX system that operates with an acceleration voltage of 20 keV. This EDX system was used to obtain the material composition of the surface region before and after the BOE etchings.

To analyze the oxygen concentration in the samples, time-of-flight secondary ion mass spectroscopy (ToF-SIMS) measurements were conducted with a TOF-SIMS M6 + system manufactured by ION-TOF, using a 30 keV pulsed Bi^{3+} primary ion beam at 45° incidence for analysis. The secondary ions generated were extracted with an O_2 gun configured at 1 keV voltage and their time-of-flight from the sample to the detector was measured by a reflection mass spectrometer. No additional surface treatment was applied prior to the ToF-SIMS measurements. Due to the complex surface morphology of the laser-textured microstructures and the absence of an absolute calibration reference, the ToF-SIMS results are discussed in terms of relative signal intensities and depth-dependent trends rather than absolute concentrations.

Optical properties of the samples were obtained by transmittance and reflectance measurements in the 200 – 2500 nm range with a Perkin-Elmer UV–Vis-NIR Lambda 1050 + spectrophotometer. A 150 mm integrating sphere was used for transmission and reflectance measurements to ensure the collection of non-specular components due to the microstructure morphology. The integrating sphere counts with a photomultiplier (for the 200 to 850 nm range) and with an InGaAs photodetector (for the 850 to 2500 nm range). Absorptance was obtained from A(%) = 100 – T(%) – R(%).

3. Results

Fig. 1, which was previously shown in reference [19], shows the typical microstructures formed on the silicon surface due to the fs-laser irradiation. The texture consists of periodical spiky quasi-conical structures with average height of ~ 18 μm and aspect ratio of 1.8 (height/width). Irregular decorations can be observed in the structure's surface. Moreover, the inset in the top-left corner shows a color image of the laser irradiated area, which presents a black coloration, due to the high light absorption, compared with the bright region around it, which corresponded with unirradiated pristine silicon.

To analyze the crystal quality of the so-called spiky silicon (SSi) samples produced by fs-laser irradiation, we first show the Raman spectroscopy results in Fig. 2. As a reference we plot the spectrum of a planar unprocessed silicon sample. To facilitate comparison, the Bare Si spectrum is multiplied by 3 due to the lower Raman intensity it presents, as it has lower absorption than the microstructured samples. The bare Si

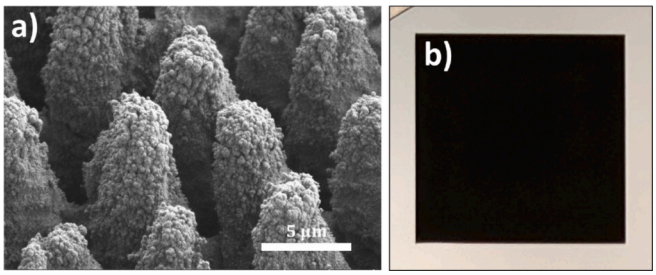

Fig. 1. A) 45° sem picture of an as-fabricated spiky silicon sample. the morphology of the fs-laser-induced texture is shown, as well as the appearance of the nano-decorations that appear on the surface of each cone. b) color photograph of the processed wafer upon specular illumination to emphasize its black coloration (processed area) in contrast to the bright background (pristine silicon wafer)[19].

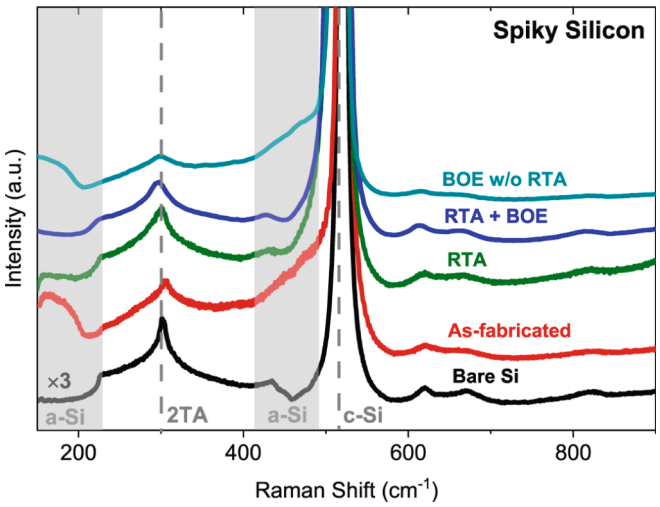

Fig. 2. Raman spectra of an unprocessed bare silicon substrate, of a SSi sample before the RTA process (as-fabricated), after the RTA process (RTA), after RTA and 1 min BOE etching (RTA + BOE), and after BOE etching for 1 min without a previous RTA (BOE w/o RTA). The bare silicon spectrum is multiplied by a factor of 3 for clarity. Dashed vertical lines indicate the main crystalline silicon modes at ~ 300 cm^{-1} (2TA second-order mode) and ~ 520 cm^{-1} (first-order crystalline Si mode), while shaded regions mark the spectral ranges associated with amorphous silicon contributions.

spectrum shows the main peak corresponding to the vibrational mode of the crystalline phase at about 520 cm^{-1} [29]. All the second-order silicon peaks can be clearly observed [30]. The second-order Raman modes are more sensitive to lack of crystallinity, since they involve two-phonon processes that require long-range order within the lattice. The most intense second-order peak, located at approximately 300 cm^{-1} corresponding to the 2TA vibrational mode, is therefore one interesting feature for evaluating differences in crystalline quality. For the as-fabricated SSi (As-fab sample) samples, the first and second crystalline-related modes are still present but with an increased signal. This is due to the much lower reflectance of the spiky microstructures which increase silicon absorptance, increasing the Raman signal. Along with the main peaks, two new bands are observed, which are attributed to the amorphous silicon extending from 400 to 520 cm^{-1}, peaking at about 480 cm^{-1} corresponding to the Si-Si stretching mode, and a low-frequency shoulder between 150 and 200 cm^{-1} associated with bending and translational vibrational modes are observed [31]. These amorphous silicon-related bands appear simultaneously with the crystalline peaks, indicating that both phases coexist within the sample. Conversely, the SSi sample postprocessed by RTA (RTA sample) does not show the amorphous bands, indicating a high lattice recrystallization. Nevertheless, the asymmetric broadening on the low-frequency side of the first order silicon peak is attributed to a decrease in crystallinity arising from defect-induced disorder [32–34]. As was expected, a selective amorphous surface SiO_x etching (RTA + BOE sample) does not alter the crystallinity of the annealed SSi sample, as indicated by the unchanged crystalline Raman vibrational modes, and the absence of the amorphous bands. Finally, samples without RTA, but etched with BOE (BOE w/o RTA sample) are quite like as-fabricated SSi samples since the amorphous related bands can be identified in both cases.

To gain insight into the structural properties of the spikes and the decorations, cross-sectional STEM images of a single spike are presented in Fig. 3. Fig. 3a displays an image of the As-fab sample. In the image we clearly distinguish the spike and the decorations, as well as some voids in the spike structure. It is interesting to note that the whole brightness of the structure is similar. Since the HAADF detector of the STEM technique is sensitive to the atomic number, this suggests that the composition of the sample shown Fig. 3a is rather homogeneous. Fig. 3b

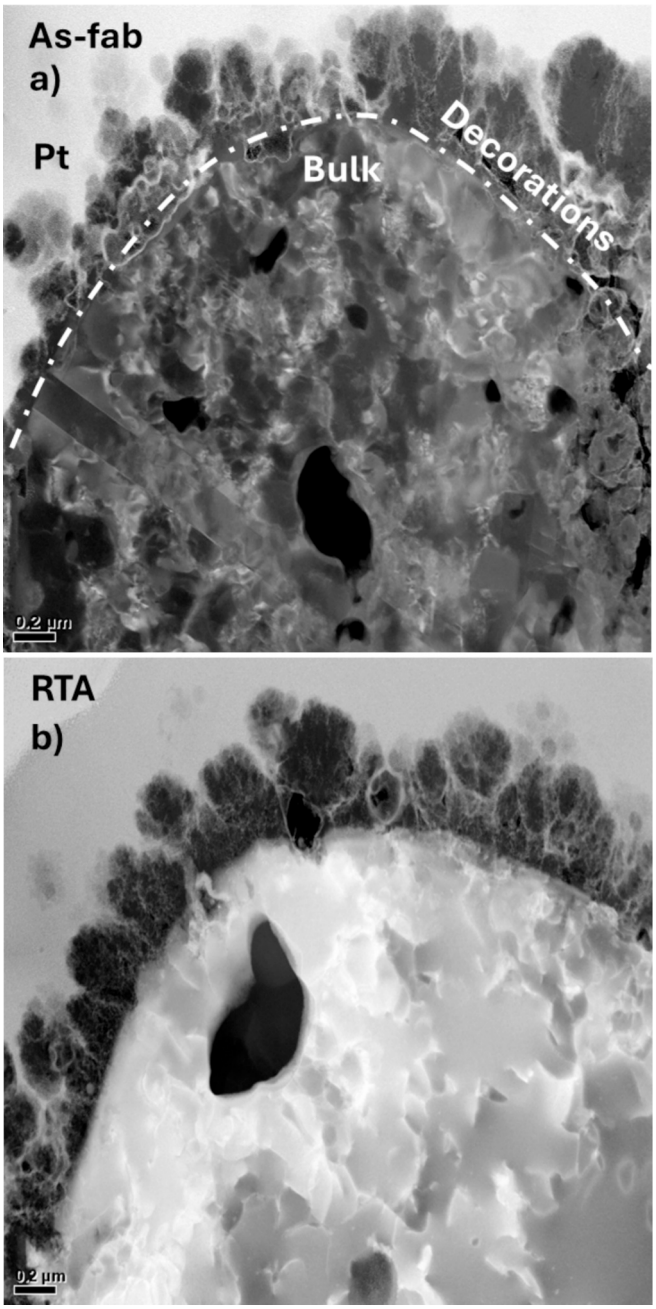

Fig. 3. STEM images of spike cross sections. (a) Sample just after femtosecond-laser processing. (b) Sample after rapid thermal annealing. The darker-contrast surface features visible in (b) correspond to the so-called "decorations". These decorations are also present in (a), more densely covering the spike surface, although they are less clearly distinguished due to contrast limitations. The scale bar is 0.2 μm.

displays the STEM image of the RTA sample. In this case, conversely to the image before the RTA process, there is a high contrast brightness for the spike and the decorations, pointing out a different composition. In fact, the atomic number of the inner part of the spike appears to be higher than in the decorations, since the brightness is higher.

As shown in Fig. 1, and Ref. [19], SSi (As-fab sample) is characterized by having small decorations at the surface of the spikes. These decorations have a thickness between 200 nm and 400 nm, approximately. We have analyzed these features in detail by means of electron microscopy. Fig. 4 shows cross-sectional TEM images in a representative region, HRTEM images from the bulk (Fig. 4a) and from the decorations/bulk

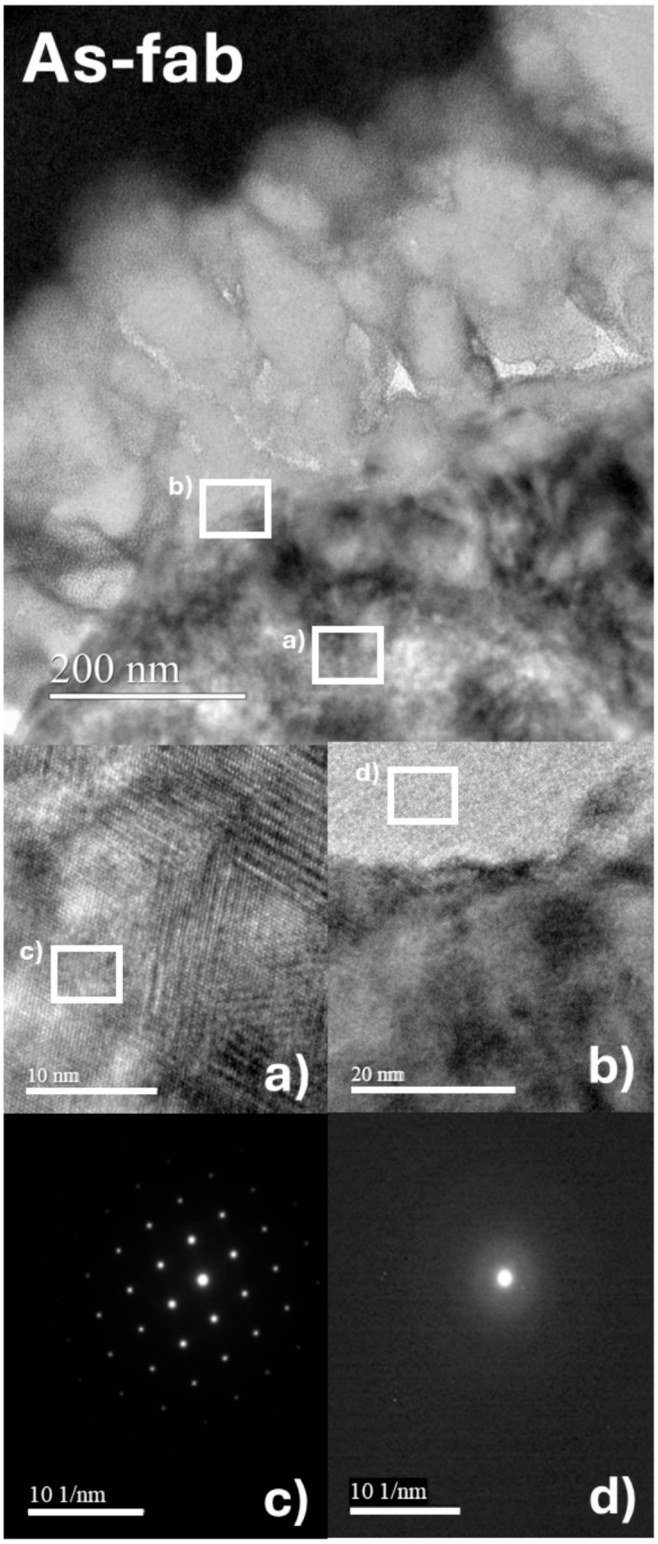

Fig. 4. TEM images of the detail of a spike cross section of the As-fab sample, showing the surface decorations. Image "a" presents an area close to the surface but below the decorations showing some defects. Image "b" presents an area containing the boundary with the decorations, showing a substrate with no visible defects. Image "c" shows the ED diffractogram of an area in the spike, well below the surface. Image "d" shows the ED diffractogram of an area containing the decorations. The regions where each image was taken are indicated with squares.

interface (Fig. 4b) and the ED patterns of these same regions (Fig. 4c. and Fig. 4d.), respectively for the As-fab sample, while Fig. 5 presents the same images for RTA sample. The morphology and bright image differences between the superficial decorations and the crystalline core structure can be differentiated clearly in the TEM images for both Figs. 4 and 5. HRTEM images of selected regions reveal a clear contrast at the boundary between the amorphous surface decorations and the single-crystalline core of the spike (Fig. 4a). The HRTEM image of a selected inner spiky microstructure region shows a region with extended defects, i.e., stacking faults, indicating lack of crystallinity produced by the laser processing (Fig. 4a). The ED pattern obtained from the inner region of the crystalline peak (Fig. 4c) exhibits well-defined spots corresponding to single-crystal silicon, in agreement with TEM observations. In contrast, the ED pattern acquired from the surface decoration area (Fig. 4d) shows a diffuse ring-like distribution typical of amorphous silicon layers [35] further supporting the TEM image identification of an amorphous structure related with the superficial decorations.

After the RTA process (Fig. 5), the cross-sectional image of the single spiky microstructure exhibits improved structural order, since the HRTEM images of the inner region do not present extended defects (Fig. 5a), even the ED related region pattern is similar to the As-fab sample for an analogous region (Fig. 5b). Moreover, the decorations exhibit different brightness than the core spike, which could indicate a different composition. The HRTEM image at the boundary between the amorphous surface decorations and the single-crystalline core of the spike (Fig. 5c) exhibits mixed crystalline and amorphous regions, which is corroborated with the mixed diffuse ring-like feature together the silicon spots (only contrast resolved for the central line) of the ED pattern in the decorated region (Fig. 4d).

To determine the compositional depth profile of the microstructures and to differentiate between the spike substrate and the decorations we plot in Fig. 6 the ToF-SIMS spectra of the main contaminants (O_2) in the silicon structure for both, the as-fabricated and the RTA samples. A pronounced increase in the oxygen signal is observed near the surface, which is attributed to the superficial decorations, while deeper regions beyond 400 nm show an almost constant oxygen concentration within the spikes. A similar trend is observed for nitrogen, although with a much lower number of counts, in agreement with previously published results (not shown) [19].

To complement the ToF-SIMS analysis and obtain more reliable information on oxygen depth distribution, EDX measurements were performed during the STEM analysis, providing quantitative information on the elemental concentrations. Fig. 7 shows EDX results for the As-fab sample (Fig. 7a), and the RTA sample (Fig. 7b). In both cases we observe a negligible nitrogen concentration (not shown), and a significant oxygen concentration in a shallow surface layer (decorations), that is strongly increased after the RTA processing.

The previous results suggest that the oxygen contained in the spikes that was introduced during the fs-laser process in air, might have migrated upon RTA to the surface to form SiO_x. We performed selective SiO_x chemical etching processes to verify if this SiO_x layer could be eliminated. Fig. 8 shows the EDX spectra of several RTA-treated SSi samples after a final BOE etching process for different etching times (1, 2, 4, 8, 16 and 32 min). The spectra show the oxygen K_α peak at about 0.525 keV which is greatly reduced after only 1 min of chemical etching (RTA + BOE sample). For longer etching times the spectra are similar (Supplementary Material, Fig. S4). As an additional result, to ensure that oxygen does not come as a result of the RTA treatment [36] a second RTA was carried out again in a sample previously annealed and etched with BOE. The oxygen peak does not present substantial differences with the RTA + BOE sample (Supplementary material).

The effect of the chemical etching on morphology of the decorations is shown in Fig. 9, where we present SEM images for two RTA-treated SSi samples, before (Fig. 9a), and after (Fig. 9b) the BOE etching process during 1 min. Moreover, a SEM image of a SSi sample only with a BOE etching but without a previous RTA (BOE w/o RTA sample) is shown

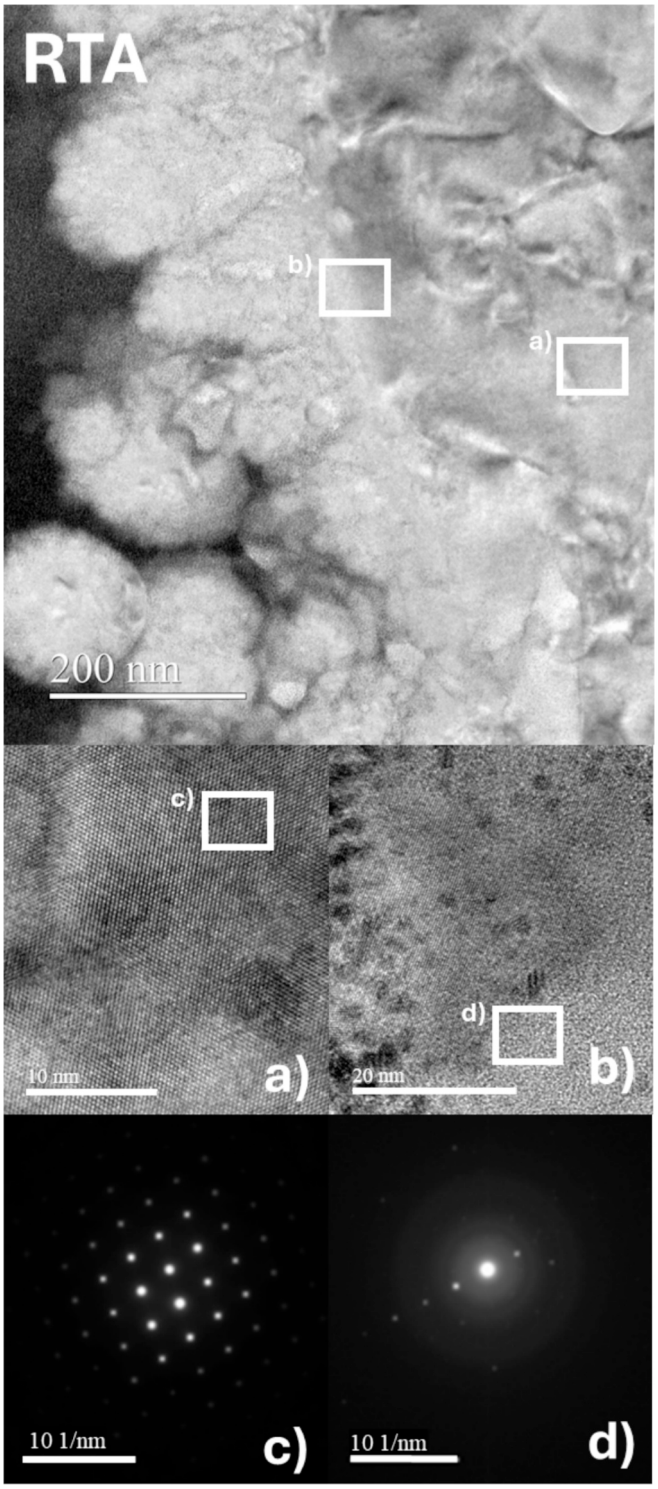

Fig. 5. TEM images of the detail of a spike cross section of the RTA sample, showing the surface decorations. Image "a" presents an area close to the surface but below the decorations showing no visible defects. Image "b" presents an area containing the boundary with the decorations, showing a monocrystalline substrate with nanocomposites. Image "c" shows the ED diffractogram of an area in the spike well below the surface. Image "d" shows the ED diffractogram of an area containing the decorations. The regions where each image was taken are indicated with squares.

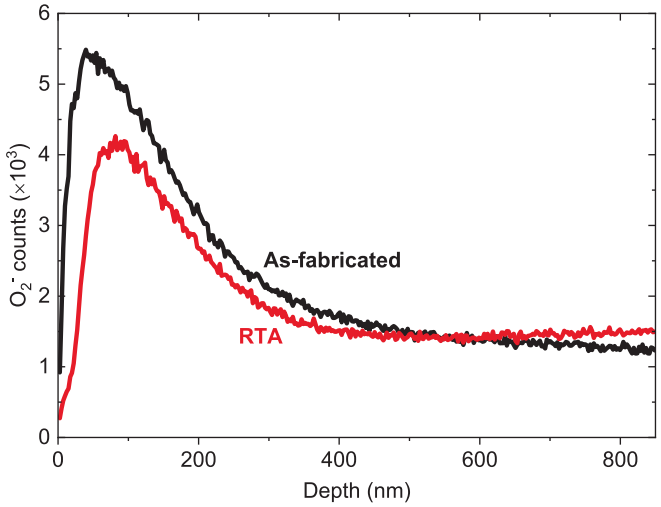

Fig. 6. ToF-SIM spectra showing the signal for O_2 as a function of depth of the As-fab sample and of the RTA sample.

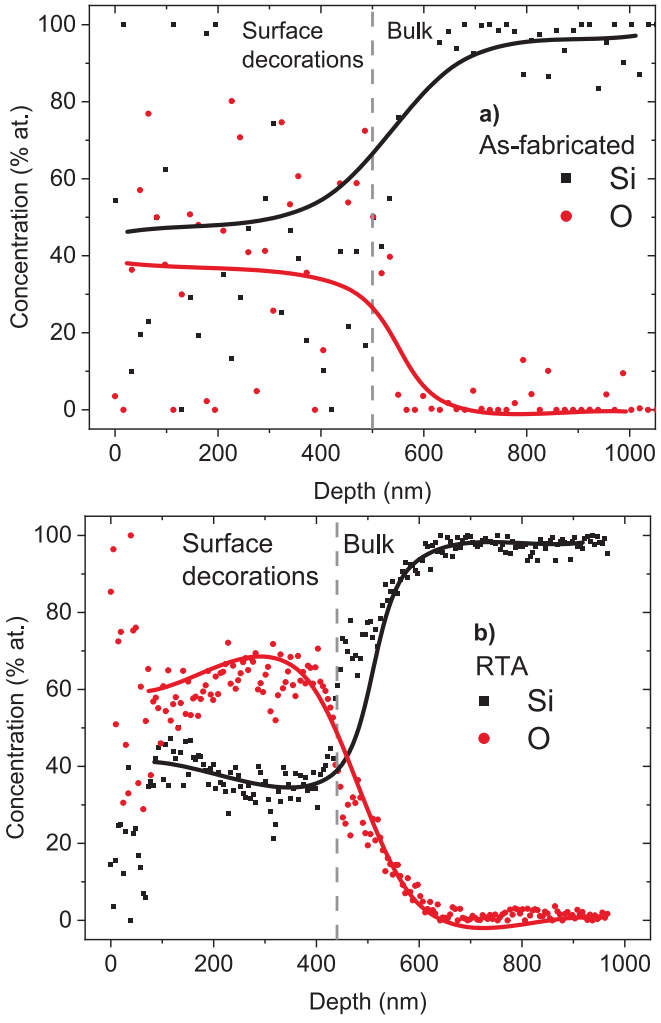

Fig. 7. EDX spectra showing the silicon and O signals for the As-fab sample (a), and for the RTA sample (b). The tendences lines are added as eye-guide. As well, the surface decorations and bulk regions are split with a vertical dashed line.

(Fig. 9c). Clearly, the etching process removes the small irregular

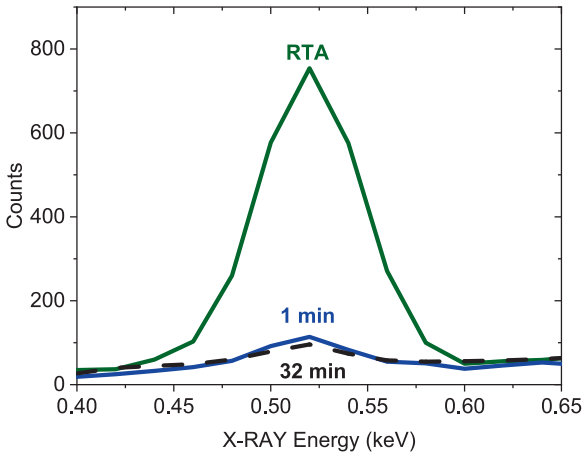

Fig. 8. EDX spectra of the surface of RTA-treated SSi samples before (green line) and after the BOE etching process during 1 min (blue line) and 32 min (black dash line).

decorations, leaving spikes with a smoother surface, regardless of whether the samples have undergone or not a previous RTA treatment.

Finally, as the main application of these SSi structures is for photovoltaic devices, we measured the absorptance of several SSi samples. Fig. 10 shows the absorptance of an unprocessed planar silicon sample for reference (Bare Si), and the As-fab, the RTA, RTA + BOE, and the BOE without RTA samples. As shown, all the SSi samples present a very high absorptance (around 95 %) in the 200 – 1000 nm range, in comparison to the lower absorptance of the reference silicon sample. At wavelengths longer than 1100 nm, all SSi samples present an increased absorptance with respect to the reference. However, since silicon cannot absorb light in this range, it has been reported that absorption is mainly originated by contaminant impurities and/or defects [37]. The As-fab sample and the BOE w/o RTA sample have no significant differences in their sub–bandgap absorptance, which shows a drop when the wavelength increases, but, after the RTA process, this absorptance is reduced to a constant value of ~ 20 %. Moreover, this constant absorption seems to be independent of the presence of decorations, because the spectra remain unaltered after the BOE etching. In highly microstructured surfaces such as spiky silicon, enhanced light trapping and multiple internal reflections can lead to lateral photon propagation and partial escape of light outside the collection solid angle of the integrating sphere. As a result, light that is neither detected as reflected nor transmitted is interpreted as absorptance by the measurement system, even in the absence of additional electronic absorption mechanisms. Similar light-trapping effects in textured silicon have been widely discussed in the literature [26].

4. Discussion

Raman spectra in Fig. 2 shows the appearance of two new bands after the fabrication of SSi samples by fs-laser irradiation in air. These bands are characteristic of amorphous silicon and disappear after RTA, which indicates the recovery of the crystallinity of the silicon lattice in the spikes. STEM images shown in Fig. 3. suggest that the crystal order is of longer range after RTA. Equally, the Z-contrast shows a different composition in both samples. As-fabricated SSi presents a quite homogenous bright between the surface spiky decorations and the spike bulk core, but after the RTA process, the sample exhibits a strong contrast, showing a dark region confined to the surface decorations and bright region outlining the spiky bulk structure. This is related to a higher concentration of light elements in the darker zones. So, based on previous works [14] and the fs-laser processing conditions, it is expected that some amount of oxygen and nitrogen have been incorporated into the material. These previous studies have shown that oxygen

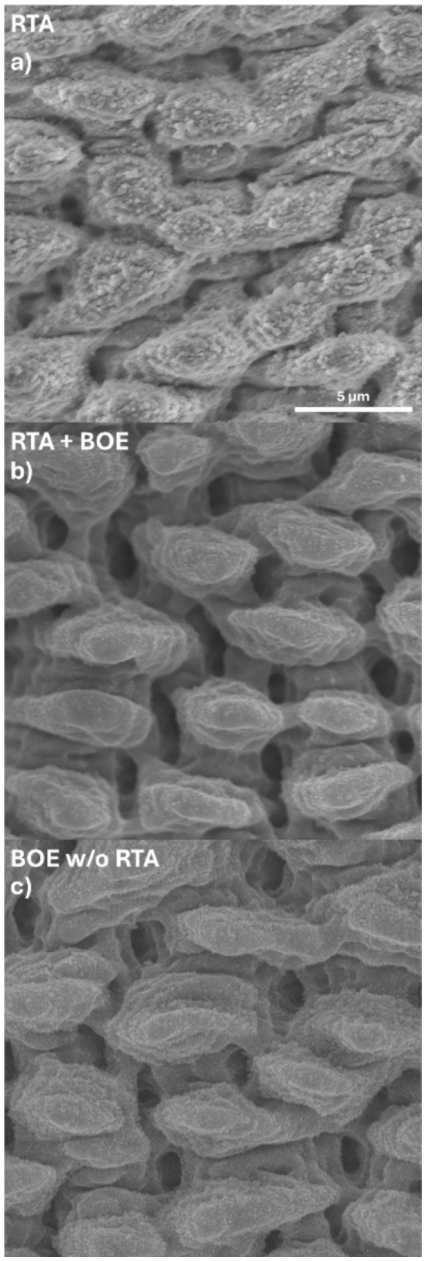

Fig. 9. Top-view SEM images of the RTA sample (a), the BOE + RTA sample (b), and the BOE w/o RTA sample (c).

incorporation during fs-laser processing can occur even under inert atmospheres and has been attributed not only to the processing environment but also to the presence of the native oxide layer on silicon surfaces. This similar contrast observed between the spike bulk region and the surface decorations in the RTA sample shows that a gathering process of the contaminating element from the bulk towards the surface is taking place during the RTA process. Moreover, STEM images (Fig. 5) show that several dark regions appear in the bulk. We may speculate that voids might have been created during the lamella's extraction with FIB. As the fs-laser process damages the internal structure of the material, other silicon phases may be formed [23,38], causing that the Ga^+ beam attacks these silicon phases more quickly than others, facilitating the creation of these voids. This idea agrees with the STEM Z–contrast images since the darker regions correspond to less dense areas. In addition, due to the different focus planes, the electron beam cannot scan the void, showing the dark region. The improvement of the crystal lattice after the RTA process is confirmed by TEM analysis. As it has been shown, the

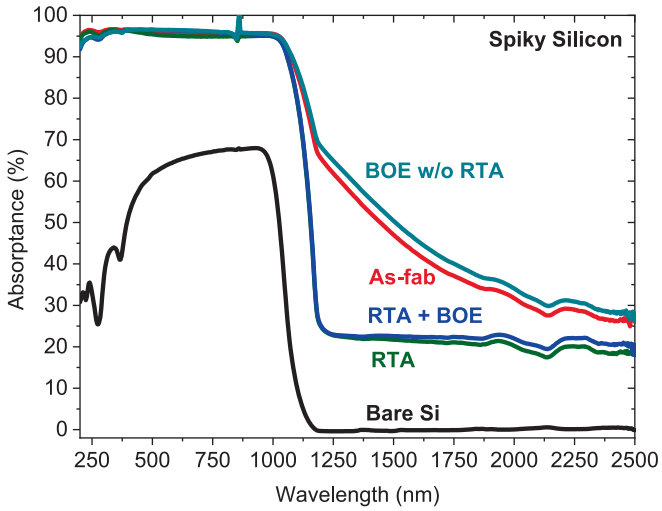

Fig. 10. Absorptance spectra of a reference bare silicon sample, as–fab sample, RTA sample, RTA + BOE sample, and BOE w/o RTA sample. The reduction of the sub-bandgap absorptance is appreciable after the RTA process.

stacking faults found in the sample after laser irradiation (Fig. 4a), disappear after RTA (Fig. 5a). The decorations themselves seem to be more crystalline: the ED diffractogram indicates that the decorations are mainly amorphous after laser irradiation (Fig. 4d), while after RTA there is some crystalline order, since some bright spots appear in Fig. 5d. Moreover, Fig. 5b contains what seem to be nano-crystalline regions, with a crystal orientation different from the one of the spike bulk. Finally, the recovery of the crystal lattice is also observed in the absorptance spectra (Fig. 10). While the samples not annealed show a high sub-bandgap absorptance due to the high quantity of defects in the material, the samples which are annealed present a lower constant sub-bandgap absorptance of ~ 20 %, which is related with an artifact in the measurement as was explained previously. As the spectra are unalterable when the BOE etching is done, and only appreciable differences appear after the RTA process, the high absorption of the unannealed samples can only be explained by defects induced during the fs-laser irradiation and not by the incorporation of contaminant.

Although different annealing temperatures and durations could be considered, previous studies on femtosecond-laser-textured silicon have shown that lower-temperature annealing often results in incomplete removal of recombination-active defects and limited recovery of electrical quality [39 40]. This motivated the use of a short-duration, high-temperature RTA approach in the present work to ensure effective structural recovery throughout the microstructures. A systematic parametric optimization of RTA conditions could be addressed in future studies.

While Raman spectroscopy and TEM analyses demonstrate substantial structural recovery after RTA, it is well established that such indicators alone do not guarantee high electrical quality in terms of minority carrier lifetime. Femtosecond-laser texturing is known to introduce recombination-active defects, and previous studies have shown that improvements in crystallinity signatures do not necessarily translate into long carrier lifetimes [41 39]. Therefore, direct lifetime measurements (e.g., QSSPC or µ-PCD) are required to fully assess the suitability of fs-laser-textured silicon for minority-carrier-based devices. Such electrical characterization will be addressed in future work.

Taken together, the structural and compositional results allow clarifying the complementary roles of the post-processing steps applied to the laser-irradiated silicon microstructures. Rapid thermal annealing has a dual effect on the laser-irradiated silicon microstructures. On one hand, it restores the crystalline lattice by removing extended defects throughout the bulk, as confirmed by Raman spectroscopy and TEM analyses. On the other hand, annealing induces a redistribution of

oxygen toward the surface, leading to the formation of oxygen-rich surface decorations, as revealed by Z-contrast STEM and EDX measurements. Subsequent buffered oxide etching selectively removes these oxide-rich decorations without altering the underlying silicon microstructures, explaining the observed compositional and morphological changes after BOE.

Another important effect observed is the incorporation of oxygen into the material during the fs-laser irradiation due to the non-controlled ambient atmosphere. Z-contrast STEM image (Fig. 3b) shows a very high contrast between the decoration and the bulk region, which indicates differences in the chemical composition of both regions. ToF-SIMS measurements (Fig. 6) demonstrate the presence of oxygen (the nitrogen contamination looks negligible) in the as-fab samples, with a higher amount of it in the first 400 nm. In this context it should be noted that the ToF-SIMS technique suffers from several drawbacks when applied to SSi samples. First, it is a spatially averaging technique with a large probing spot size, thus yielding an average result over multiple spikes and decorations. Second, ToF–SIMS suffers from the "beam-mixing" effect [42], which means that there is a certain maximum slope for a profile that can be resolved, being this another kind of averaging. Finally, and probably more important, since the spikes microstructure is very uneven, results are being extracted at the same time from the decorations and from the spikes when the measurement is evolving. All these effects can produce a similar average oxygen concentration for both samples even if at a nanometric scale they are different. The EDX analysis over the cross-sectional samples prepared for STEM, adds more information about the distribution of oxygen in the structures. Fig. 7 shows an increase of oxygen in the 600 nm upper layer for the as-fabricated SSi. However, after RTA, the increase in the oxygen concentration is more clearly detected and limited to the upper 400 nm, which coincides with the area of the decorations. It should be noted that the very near-surface region (first ~ 100 nm) is influenced by the lamella preparation and the presence of the Pt protective layer used during FIB milling, which can locally affect the apparent elemental ratios in the EDX profiles. Therefore, the discussion of oxygen redistribution focuses on the surface decoration region rather than on the immediate interface. Beyond this interface, the EDX data clearly indicate that after RTA the oxygen is preferentially concentrated in the decoration layer, while the deeper bulk exhibits a reduced and more homogeneous oxygen distribution compared to the as-fabricated sample. This difference clearly shows the oxygen gathering effect that we propose. Even more, the silicon oxide formed in the decorations after RTA resembles a more stoichiometric compound because of the 1:2 ratio between the silicon and oxygen atomic concentration.

As the surface decorations are composed of SiO_2 after RTA, a selective etching can remove these structures without modifying the spike morphology. As shown in Fig. 2, the BOE etching does not affect the crystalline silicon structure, because the spectra of the etched samples look like that of their homologous but without the BOE etching. This is expected because the SiO_x decorations do not absorb the green excitation wavelength at 532 nm of the Raman laser used, so the amorphous nature of the SiO_x decorations cannot be detected in the Raman spectra. The EDX spectra in Fig. 7 shows that an etching with the buffered BOE solution for 1 min is enough to remove the oxygen content at the spike surface. The difference between the samples before and after BOE etching can be observed in the SEM images (Fig. 9), where the samples that were etched show a smoother surface without decorations compared to the sample without BOE etching, even without RTA. This analysis is in agreement with the absorptance results of Fig. 10, where after the chemical etching, the absorptance spectra remain unalterable due to the wide bandgap of SiO_x, so the wavelengths measured in the absorption analysis are not absorbed by the superficial SiO_x decorations.

Finally, regarding the optical properties of the samples shown in Fig. 10, it is known that the extremely high absorptance measured at wavelengths below 1100 nm is mainly produced by multiple reflections of the spikes. However, silicon cannot absorb wavelengths above 1100 nm unless defects and/or impurities were presented in the material. Since no impurities were intentionally introduced into the material, apart from the elements present in the air atmosphere, the sub-band gap absorption observed in Fig. 10, for SSi samples can be attributed to intrinsic defects in the crystal lattice and/or contaminant elements. It can be clearly seen that the RTA process reduces the sub-bandgap absorption to a constant value of ~ 20 %, related with a measurement artifact as it has been previously said, so the defects in the crystal lattice which produce the absorption have been removed. Even more, the absorption spectrum seem unaltered when the BOE etching is performed, indicating that the presence of oxygen in the material do not play a role in the sub-bandgap absorption. Finally, the absorption under the bandgap energy is unchanged when the RTA and/or the BOE etching are performed, so the structure of the spikes does not change due to these treatments.

Several strategies have been proposed to reduce recombination-active defects in femtosecond-laser and microtextured silicon while maintaining high optical absorptance [43]. One approach relies on tailoring laser parameters to minimize subsurface damage, although this often involves a trade-off between absorptance and electrical quality [44]. Alternatively, post-laser treatments such as thermal annealing, surface etch-back, and passivation have been shown to significantly improve minority carrier lifetime by removing damaged regions and recombination-active defects [39]. In this context, the combination of RTA and BOE approach presented here offers a complementary strategy, enabling the removal of extended crystalline defects together with the selective elimination of oxide-rich surface decorations [41]. While this structural and compositional recovery is a necessary step toward high electrical quality, direct lifetime measurements are required for a quantitative comparison with previously reported approaches.

From a process-integration perspective, the proposed approach relies on unit operations that are largely compatible with standard semiconductor fabrication workflows. RTA in inert atmosphere and buffered oxide etching are well-established wafer-level processes routinely implemented using industrial equipment and therefore do not impose intrinsic limitations on scalability. The primary constraint in scaling the overall process arises from the femtosecond-laser texturing step, which is inherently based on serial scanning. However, processing in ambient air, without vacuum or controlled atmospheres, combined with galvanometric scanning, significantly reduces process complexity compared to alternative approaches. Further improvements in throughput may be achieved through high-repetition-rate laser sources and optimized scan strategies, although quantitative throughput analysis is beyond the scope of this work.

5. Conclusions

In this work we introduce a key step to enhance the material performance of SSi obtained by fs-laser processing in air. It consists in a RTA process in an inert atmosphere followed by a selective SiO_2 etching, to enhance the material performance of SSi obtained. Based on our previous study, optimal conditions were chosen for the laser-fabrication of the spikes, which yielded to high absorptance and a large aspect ratio of the spikes. The obtained material shows some defects that allow the absorption of photons below the silicon bandgap energy. These defects are present in the bulk and the surface features decorations of amorphous silicon. The use of air and the presence of the native oxide at the silicon surface allow the introduction of oxygen into the material during the fs-laser fabrication process. Most crystalline defects induced in the fabrication have been removed with RTA treatments, which, in addition, produces a gathering of the oxygen introduced during the fs-laser processing from the bulk to the surface decorations, that are oxidized to form SiO_x. Then, a selective etching with a buffered hydrofluoric solution was performed to remove the oxidized surface decorations. Finally, the material obtained shows a high absorptance (around ~ 95 %) in the range between 200 and 1100 nm. This way we have obtained a

crystalline, defect-free material with a clean microtextured surface and high light absorption that can be modified to be used in optoelectronics devices, such as solar cells or IR detectors, with minimal changes in the manufacturing route.

CRediT authorship contribution statement

Rafael Benítez-Fernández: Writing – original draft, Methodology, Investigation, Formal analysis, Data curation, Conceptualization. **Gonzalo Gomez-Munoz:** Writing – review & editing, Writing – original draft, Investigation, Formal analysis, Data curation, Conceptualization. **Eric García-Hemme:** Project administration, Funding acquisition. **Núria Roca–Giménez:** Writing – review & editing, Investigation. **Fátima Cabello:** Writing – review & editing, Investigation. **Marina García-Pardo:** Writing – review & editing, Investigation. **Jose Gonzalo:** Writing – review & editing, Supervision, Project administration, Investigation, Funding acquisition, Conceptualization. **Javier Solis:** Writing – review & editing, Supervision, Project administration, Investigation, Funding acquisition, Conceptualization. **Álvaro del Prado:** Writing – review & editing, Supervision, Project administration. **Mario Garcia-Lechuga:** Writing – review & editing, Supervision, Investigation, Conceptualization. **Javier Olea:** Writing – review & editing, Writing – original draft, Supervision, Project administration, Funding acquisition. **Jan Siegel:** Writing – review & editing, Writing – original draft, Supervision, Project administration, Investigation, Funding acquisition, Formal analysis, Data curation, Conceptualization. **David Pastor:** Writing – review & editing, Writing – original draft, Supervision, Project administration, Investigation, Funding acquisition, Formal analysis, Data curation, Conceptualization.

Declaration of competing interest

The authors declare the following financial interests/personal relationships which may be considered as potential competing interests: [Rafael Benitez Fernandez, Gonzalo Gomez Munoz, Eric Garcia Hemme, Nuria Roca Gimenez, Fatima Cabello, Marina Garcia Pardo, Jose Gonzalo, Javier Solis, Alvaro del Prado, Mario Garcia Lechuga, Javier Olea, Jan Siegel, David Pastor reports financial support was provided by Spain Ministry of Science Innovation and Universities. Rafael Benitez Fernandez, Eric Garcia Hemme, Nuria Roca Gimenez, Alvaro del Prado, Javier Olea, David Pastor reports financial support was provided by Community of Madrid. Rafael Benitez Fernandez, Gonzalo Gomez Munoz, Jose Gonzalo, Javier Solis, Javier Olea, David Pastor has patent pending to P202531047. Rafael Benitez Fernandez, Gonzalo Gomez Munoz, Jose Gonzalo, Javier Solis, Javier Olea, David Pastor has patent pending to U202532258. If there are other authors, they declare that they have no known competing financial interests or personal relationships that could have appeared to influence the work reported in this paper].

Acknowledgements

This work has been supported by grant HyperSolar (TED2021130894B-C21 and TED2021-130894B-C22) funded by MICIU/AEI/ 10.13039/501100011033 and by the European Union NextGenerationEU/PRTR, grant HyperSpec (PID2023-148178OB-C21 and PID2023-148178OB-C22) funded by MICIU/AEI/10.13039/501100011033 and by ERDF/EU, grant MATRIX-CM ((TEC-2024/TEC-85), funded by Consejería de Educacion, Ciencia y Universidades (Comunidad de Madrid, (Spain)). The support of the Regional Government of Madrid through the Project 4EVERPV-CM (TEC-2024/ECO-72) is acknowledged. This work was partially supported by the Spanish Research Agency (AEI, Ministry of Research and Innovation) and the European Regional Development Fund (ERDF) under grants PID2020-116508RB-I00 and PID2020–117498RB-I00. R. Benítez-Fernández acknowledges the predoctoral contract from Comunidad Autónoma de Madrid (PIPF-2023/ECO-30541). Authors want to acknowledge assistance from CAI de Técnicas Químicas (Espectroscopía Raman y Correlación) for the Raman measurements and CAI de Técnicas Físicas (Implantación Iónica) from the Universidad Complutense de Madrid for the RTA processes. We also acknowledge ICTS-CNME (Madrid, Spain) for the SEM, TEM and STEM images, EDS and EDX characterization. Authors also acknowledge Servicio de Nanotecnología y Análisis de Superficies del CACTI de la Universidad de Vigo for ToF-SIMS measurements. Authors acknowledge the use of instrumentation as well as the technical advice provided by the National Facility ELECMI ICTS, node "Laboratorio de Microscopías Avanzadas" at University of Zaragoza.

Appendix A. Supplementary data

Supplementary data to this article can be found online at https://doi.org/10.1016/j.apsusc.2026.166323.

Data availability

Data will be made available on request.

References

[1] T.H. Her, R.J. Finlay, C. Wu, S. Deliwala, E. Mazur, Microstructuring of silicon with femtosecond laser pulses, Appl. Phys. Lett. 73 (12) (1998) 1673–1675, https://doi.org/10.1063/1.122241.
[2] C.H. Hsu, J.R. Wu, Y.T. Lu, D.J. Flood, A.R. Barron, L.C. Chen, Fabrication and characteristics of black silicon for solar cell applications: an overview, Mater. Sci. Semicond. Process. 25 (2014) 2–17, https://doi.org/10.1016/J.MSSP.2014.02.005.
[3] B.R. Tull, J.E. Carey, E. Mazur, J.P. McDonald, S.M. Yalisove, Silicon surface morphologies after femtosecond laser irradiation, MRS Bull. 31 (8) (2006) 626–633, https://doi.org/10.1557/MRS2006.160.
[4] V.V. Iyengar, B.K. Nayak, M.C. Gupta, Optical properties of silicon light trapping structures for photovoltaics, Sol. Energy Mater. Sol. Cells 94 (12) (2010) 2251–2257, https://doi.org/10.1016/J.SOLMAT.2010.07.020.
[5] C.F. Baron, et al., Biomimetic surface structures in steel fabricated with femtosecond laser pulses: influence of laser rescanning on morphology and wettability, Beilstein J. Nanotechnol. 9 (1) (2018) 2802–2812, https://doi.org/10.3762/BJNANO.9.262.
[6] Z. Zhao, et al., Black silicon for near-infrared and ultraviolet photodetection: a review, APL Mater. vol. 11 (2) (2023), https://doi.org/10.1063/5.0133770/2870955.
[7] E. Stratakis, et al., Laser engineering of biomimetic surfaces, Materials Science and Engineering: R: Reports 141 (2020) 100562, https://doi.org/10.1016/J.MSER.2020.100562.
[8] M.K. Basher, M.K. Hossain, M.J. Uddin, M.A.R. Akand, K.M. Shorowordi, Effect of pyramidal texturization on the optical surface reflectance of monocrystalline photovoltaic silicon wafers, Optik (stuttg) 172 (2018) 801–811, https://doi.org/10.1016/J.IJLEO.2018.07.116.
[9] M. Valiei, P.M. Shaibani, H. Abdizadeh, M. Kolahdouz, E. Asl Soleimani, J. Poursafar, Design and optimization of single, double and multilayer anti-reflection coatings on planar and textured surface of silicon solar cells, Mater. Today Commun. 32 (2022), https://doi.org/10.1016/J.MTCOMM.2022.104144.
[10] B. Franta, E. Mazur, S.K. Sundaram, Ultrafast laser processing of silicon for photovoltaics, Int. Mater. Rev. 63 (4) (2018) 227–240, https://doi.org/10.1080/09506608.2017.1389547/ASSET/D7EC235B-A78B-473F-A34D-9510ACB53FF3/ASSETS/IMAGES/LARGE/10.1080_09506608.2017.1389547-FIG14.JPG.
[11] E. Hvidsten Dahl, J. Madsbøll, A.K. Søiland, J.O. Odden, R. Tronstad, A. Nylandsted Larsen, Electrically active sodium-related defect centres in silicon, Semicond. Sci. Technol. vol. 28 (10) (2013), https://doi.org/10.1088/0268-1242/28/10/105010.
[12] A.R. Martin, M. Baeyens, W. Hub, P.W. Mertens, B.O. Kolbesen, Alkaline cleaning of silicon wafers: additives for the prevention of metal contamination, Microelectron. Eng. 45 (2–3) (1999) 197–208, https://doi.org/10.1016/S0167-9317(99)00150-1.
[13] A. Luque, A. Martí, E. Antolín, C. Tablero, Intermediate bands versus levels in non-radiative recombination, Physica B Condens. Matter 382 (1–2) (2006) 320–327, https://doi.org/10.1016/j.physb.2006.03.006.
[14] R. Younkin, J.E. Carey, E. Mazur, J.A. Levinson, C.M. Friend, Infrared absorption by conical silicon microstructures made in a variety of background gases using femtosecond-laser pulses, J. Appl. Phys. 93 (5) (2003) 2626–2629, https://doi.org/10.1063/1.1545159.
[15] G. Nava, et al., Scaling of black silicon processing time by high repetition rate femtosecond lasers, Optical Materials Express. 3 (5) (2013) 612–623, https://doi.org/10.1364/OME.3.000612.
[16] Z. Wen, et al., Large-scale wideband light-trapping black silicon textured by laser inducing assisted with laser cleaning in ambient air, Nanomaterials 12 (10) (2022) 1772, https://doi.org/10.3390/NANO12101772.

[17] Y. Peng, Y. Zhou, X. Chen, Y. Zhu, The fabrication and characteristic investigation of microstructured silicon with different spike heights, Opt. Commun. 334 (2015) 122–128, https://doi.org/10.1016/J.OPTCOM.2014.08.034.
[18] M.Y. Shen, C.H. Crouch, J.E. Carey, E. Mazur, Femtosecond laser-induced formation of submicrometer spikes on silicon in water, Appl. Phys. Lett. 85 (23) (2004) 5694–5696, https://doi.org/10.1063/1.1828575.
[19] G. Gomez-Munoz, et al., Tuning spike-like morphologies in Silicon by sustainable fs-laser processing in air for enhanced light absorption, Appl. Surf. Sci. 686 (2025) 161967, https://doi.org/10.1016/J.APSUSC.2024.161967.
[20] K. Werner, et al., Single-shot multi-stage damage and ablation of silicon by femtosecond mid-infrared laser pulses, Sci. Rep. 9 (1) (2019) 1–13, https://doi.org/10.1038/S41598-019-56384-0;SUBJMETA.
[21] R. Zhang, C. Huang, J. Wang, S. Feng, H. Zhu, Evolution of micro/nano-structural arrays on crystalline silicon carbide by femtosecond laser ablation, Mater. Sci. Semicond. Process. 121 (2021) 105299, https://doi.org/10.1016/J.MSSP.2020.105299.
[22] Y. Liu, et al., Research on monocrystalline silicon micro-nano structures irradiated by femtosecond laser, Materials vol. 15 (14) (2022) 4897, https://doi.org/10.3390/MA15144897.
[23] J.H. Zhao, X.B. Li, Q.D. Chen, Z.G. Chen, H.B. Sun, Ultrafast laser-induced black silicon, from micro-nanostructuring, infrared absorption mechanism, to high performance detecting devices, Mater. Today Nano 11 (2020) 100078, https://doi.org/10.1016/J.MTNANO.2020.100078.
[24] J. Jiang, S. Li, Y. Jiang, Z. Wu, Z. Xiao, Y. Su, Mechanism of optical absorption enhancement of surface textured black silicon, J. Mater. Sci. Mater. Electron. 24 (2) (2013) 463–466, https://doi.org/10.1007/S10854-012-0756-Z/FIGURES/4.
[25] H. Nussbaumer, G. Willeke, E. Bucher, Optical behavior of textured silicon, J. Appl. Phys. 75 (4) (1994) 2202–2209, https://doi.org/10.1063/1.356282.
[26] P. Campbell, M.A. Green, Light trapping properties of pyramidally textured surfaces, J. Appl. Phys. 62 (1) (1987) 243–249, https://doi.org/10.1063/1.339189.
[27] C. Florian, et al., Single femtosecond laser-pulse-induced superficial amorphization and re-crystallization of silicon, Materials. 14 (7) (2021) 1651, https://doi.org/10.3390/MA14071651.
[28] J.M. Liu, Simple technique for measurements of pulsed Gaussian-beam spot sizes, Opt. Lett. 7 (5) (1982) 196–198, https://doi.org/10.1364/OL.7.000196.
[29] J.H. Parker, D.W. Feldman, M. Ashkin, Raman scattering by silicon and germanium, Phys. Rev. 155 (3) (1967) 712, https://doi.org/10.1103/PhysRev.155.712.
[30] P.A. Temple, C.E. Hathaway, Multiphonon raman spectrum of silicon, Phys. Rev. B 7 (8) (1973) 3685, https://doi.org/10.1103/PhysRevB.7.3685.
[31] D. Bermejo, M. Cardona, Raman scattering in pure and hydrogenated amorphous germanium and silicon, J. Non Cryst. Solids 32 (1–3) (1979) 405–419, https://doi.org/10.1016/0022-3093(79)90085-1.
[32] A. Zwick, R. Carles, Multiple-order Raman scattering in crystalline and amorphous silicon, Phys. Rev. B 48 (9) (1993) 6024, https://doi.org/10.1103/PhysRevB.48.6024.
[33] R.F. Wood, D.H. Lowndes, G.E. Jellison, F.A. Modine, Melting model and Raman scattering during pulsed laser annealing of ion-implanted silicon, Appl. Phys. Lett. 41 (3) (1982) 287–290, https://doi.org/10.1063/1.93467.
[34] I.H. Campbell, P.M. Fauchet, The effects of microcrystal size and shape on the one phonon Raman spectra of crystalline semiconductors, Solid State Commun. 58 (10) (1986) 739–741, https://doi.org/10.1016/0038-1098(86)90513-2.
[35] H. Hofmeister, J. Dutta, H. Hofmann, Atomic structure of amorphous nanosized silicon powders upon thermal treatment, Phys. Rev. B 54 (4) (1996) 2856, https://doi.org/10.1103/PhysRevB.54.2856.
[36] B. Mohadjeri, M.R. Baklanov, E. Kondoh, K. Maex, Oxidation and roughening of silicon during annealing in a rapid thermal processing chamber, J. Appl. Phys. 83 (7) (1998) 3614–3619, https://doi.org/10.1063/1.366629.
[37] N.D. Cuong, J. Blair, Impurity photovoltaic effect in cadmium sulfide, J. Appl. Phys. 37 (4) (1966) 1660–1669, https://doi.org/10.1063/1.1708581.
[38] Z. Sun, M.C. Gupta, Laser processing of silicon for photovoltaics and structural phase transformation, Appl. Surf. Sci. 456 (2018) 342–350, https://doi.org/10.1016/J.APSUSC.2018.06.092.
[39] X. Liu, et al., Millisecond-level minority carrier lifetime in femtosecond laser-textured black silicon, IEEE Photon. Technol. Lett. 34 (16) (2022) 870–873, https://doi.org/10.1109/LPT.2022.3190270.
[40] B. Radfar, et al., "Extended infrared absorption in nanostructured Si through se implantation and flash lamp annealing", Physica Status Solidi (A) Applications and Materials Science. vol. 221 (24) (2024) 2400133 https://doi.org/10.1002/PSSA.202400133; WGROUP:STRING:PUBLICATION.
[41] V. Vähänissi, K. Chen, H. Savin, B. Radfar, O.E. Setälä, X. Liu, Optoelectronic properties of black silicon fabricated by femtosecond laser in ambient air: exploring a large parameter space, Opt. Lett. 48 (5) (2023) 1224–1227, https://doi.org/10.1364/OL.481890.
[42] T. Grehl, R. Möllers, E. Niehuis, Low energy dual beam depth profiling: influence of sputter and analysis beam parameters on profile performance using TOF-SIMS, Appl. Surf. Sci. 203–204 (2003) 277–280, https://doi.org/10.1016/S0169-4332(02)00653-0.
[43] X. Liu, et al., Perspectives on black silicon in semiconductor manufacturing: experimental comparison of plasma etching, MACE, and Fs-laser etching, IEEE Trans. Semicond. Manuf. 35 (3) (2022) 504–510, https://doi.org/10.1109/TSM.2022.3190630.
[44] X. Liu, B. Radfar, K. Chen, T.P. Pasanen, V. Vähänissi, H. Savin, Tailoring femtosecond-laser processed black silicon for reduced carrier recombination combined with >95% above-bandgap absorption, Adv. Photonics Res. 3 (4) (2022) 2100234, https://doi.org/10.1002/ADPR.202100234.